Audio Engineering Society

Convention Paper

Presented at the 120th Convention
2006 May 20–23 Paris, France

3D Sound Field Recording with Higher Order Ambisonics – Objective Measurements and Validation of a 4th Order Spherical Microphone

Sébastien Moreau[1], Jérôme Daniel[2], and Stéphanie Bertet[2]

[1] 23/25 boulevard Edgard Quinet, 92700 Colombes, France
moreau-sebastien@ifrance.com

[2] France Telecom R&D, 2 avenue Pierre Marzin, 22307 Lannion Cedex, France
jerome.daniel@francetelecom.com, stephanie.bertet@francetelecom.com

ABSTRACT

Higher Order Ambisonics (HOA) is a flexible approach for representing and rendering 3D sound fields. Nevertheless, lack of effective microphone systems limited its use until recently. As a result of authors' previous work on the theory and design of spherical microphone arrays, a 4th order HOA microphone has been built, measured and used for natural recording. The present paper first discusses theoretical aspects and physical limitations proper to discrete, relatively small arrays (spatial aliasing, low-frequency estimation). Then it focuses on the objective validation of such microphones. HOA directivities reconstructed from simulated and measured 3D responses are compared to the expected spherical harmonics. Criteria like spatial correlation help characterizing the encoding artifacts due to the model limitations and the prototype imperfections. Impacts on localisation criteria are evaluated.

1. INTRODUCTION

Ambisonics is a 3D sound spatialisation technology developed mostly by Michael Gerzon [1] in the early 1970s, which permits to render 3D sound fields in a flexible way from the knowledge of their 1st order directive information at one point: omnidirective (W) and 3D bidirective (X, Y, Z) components which constitute the so-called B-Format . Nevertheless, its low spatial resolution limits the correct sound field reconstruction to a small listening area, especially for high frequencies. Higher Order Ambisonics (HOA) [2-4] extends the B-Format to higher resolution by means of spherical harmonic decomposition of the sound field, which results in enlarging the reproduction area (*i.e.* the sweet spot).

A practical 1st order HOA recording system was described from the very beginning by Craven and Gerzon [5], from which the so-called SoundField microphone was built. Nevertheless, until recently physical limitations of small discrete microphone arrays didn't make possible the implementation of HOA pickup systems with higher spatial resolution. Authors'

previous work and other recent studies brought practical solutions to design such microphone arrays. Different strategies have been proposed, including spherical microphone arrays [6-12] and arrays with multiple radii [13].

After reviewing HOA basics, the present paper focuses on the objective validation of spherical microphones arrays for HOA recording. Theoretical aspects of discrete sensor arrays are discussed and highlight physical limitations proper to relatively small discrete arrays, especially concerning spatial aliasing and low frequency estimation. The latter involves filters with excessive bass-boost which need to be reduced for practical purpose. This is done by introducing regularization filters in the estimation process. Finally, a 4th order prototype have been built, measured and used for natural recording for objective validation of such microphones. HOA directivities reconstructed from simulated and measured 3D responses are compared to the expected spherical harmonics. Criteria like spatial correlation help characterizing the encoding artifacts due to the model limitations and the prototype imperfections.

2. HIGHER ORDER AMBISONICS BASICS

This section draws a brief overview of basic concepts and properties of HOA. Before introducing further acoustics fundamentals in 2.2, we first restrain to horizontal systems description in 2.1. All concepts introduced in this section are more thoroughly discussed and extended to 3D in [3, 14]. They are useful as a starting point for the problematic of HOA recording. They also provide complementary characterisation criteria to asses the microphone performance from the reproduction point of view.

2.1. Spatial encoding and decoding for virtual sound imaging

Ambisonics can be categorized in the family of amplitude panning techniques, when dealing with virtual source spatialisation, and/or coincident microphone techniques when dealing with sound field recording. Among them Ambisonics has the particularity of splitting the spatialisation process into spatial encoding and spatial decoding.

2.1.1. Spatial encoding

Spatial encoding itself is a kind of amplitude pan-pot but results in an intermediary format that is not dedicated to any loudspeaker setup for sound reproduction. Equations system (1) shows encoding laws for a source in azimuth direction θ_v and emitting a signal S_v:

$$\begin{aligned} W &= B_{00}^{+1} = 1.S_v \\ X &= B_{11}^{+1} = \sqrt{2}\cos\theta_v.S_v \\ Y &= B_{11}^{-1} = \sqrt{2}\sin\theta_v.S_v \\ &\vdots \\ B_{mm}^{+1} &= \sqrt{2}\cos m\theta_v.S_v \\ B_{mm}^{-1} &= \sqrt{2}\sin m\theta_v.S_v \\ &\vdots \end{aligned} \qquad (1)$$

The first three lines define the so-called "1st order horizontal encoding" and yield the horizontal components (W,X,Y) of the well-known B-Format introduced by Gerzon [15]. For each new "*order*" m>1 up to a maximum order M, a pair of additional lines exhibits Higher Order Ambisonics encoding functions and associated components B_{mm}^{σ}. Note that the order m corresponds to the angular frequency. An M^{th} order 2D sound field representation comprises (2M+1) components.

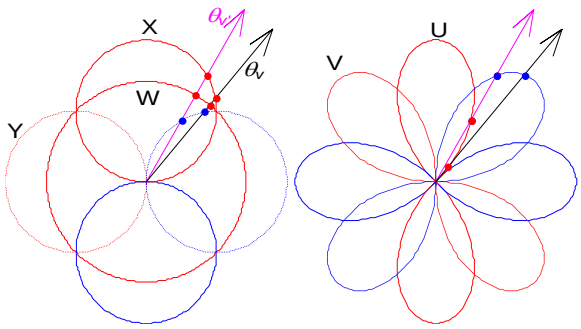

Figure 1 Horizontal encoding using 0th, 1st order (left) and 2nd order (right) directivity patterns. Positive and negative gains are resp. in red and blue. For each source (in arrow's direction) and each directivity, the encoding gain is given by the intersection point between arrow and pattern (more precisely its distance from the centre).

As illustrated on the left part of Figure 1, 1st order encoding offers a quite limited angular discrimination for virtual sources that are relatively close to each other. This is probably a first cause of the lack of sound image

precision and robustness criticized by detractors of Ambisonics (and of coincident microphone techniques more generally). By introducing "higher order ambisonic" encoding functions (1), *i.e.* functions which variation is greater for the same angular variation, a better angular discrimination is possible (right part of Figure 1 illustrates encoding with 2nd order functions).

Left column of Figure 3 shows polar patterns of ambisonics directivities up to the 4th order. Since 1st order recording requires omni and bidirectional microphones, or a combination of *e.g.* cardioids, it easily makes sense for sound engineers. The latter might be dubious regarding practical recording using higher order directivities since no existing single microphone has one of such directivities. It is the object of this paper to prove that an efficient solution exists.

2.1.2. Spatial decoding

Generally speaking, spatial decoding consists in combining ambisonic signals B_{mm}^{σ} to produce signals S_n radiated by loudspeakers, with the aim at creating phantom sound images accordingly to the encoded sound scene. More formally, this is done by a matrix operation:

$$\mathbf{s} = \mathbf{D}.\mathbf{b}, \qquad (2)$$

exhibiting decoding matrix $\mathbf{D}$ and vectors $\mathbf{s} = [S_1 \dots S_N]$ and $\mathbf{b} = \left[B_{00}^{+1}\ B_{11}^{+1}\ B_{11}^{-1} \dots B_{MM}^{+1}\ B_{MM}^{-1} \right]$. We qualify as "basic" the decoding such that the ambisonic sound field that would be recorded in the centre of loudspeakers setup is the same as the originally encoded sound field [16]. In the case where loudspeakers form a regular polygon and with encoding convention of (1), decoding matrix is defined as:

$$\mathbf{D} = \frac{1}{N}\mathbf{C}^T, \qquad (3)$$

where columns of matrix $\mathbf{C} = [\mathbf{c}_1 \dots \mathbf{c}_N]$ are vectors $\mathbf{c}_n = \left[1 \dots \sqrt{2}\cos(M\theta_n)\ \sqrt{2}\sin(M\theta_n)\right]^T$ of encoding gains associated to loudspeaker azimuth θ_n. For an M^{th} order encoding, at least N=2M+2 loudspeakers are recommended for a homogeneous reproduction.

Another way of understanding ambisonic spatialization is to merge spatial encoding and decoding, so that encoding directivities are themselves combined to form directivities of virtual microphones associated to loudspeakers individually, as if these virtual microphones would directly capture the sound field and feed the loudspeakers (Figure 2).

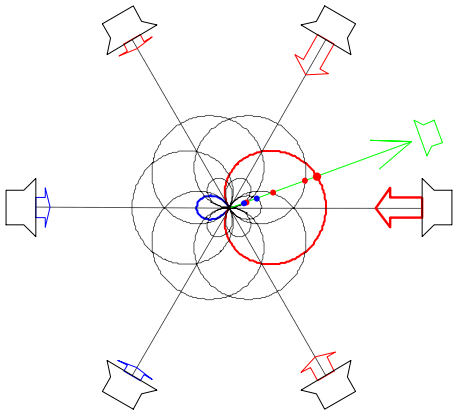

Figure 2 Virtual recording equivalent to 1st order encoding and basic decoding over a hexagonal layout, with a sub-cardioid pointing to each loudspeaker (only one is coloured for clarity). For each loudspeaker and for a given direction virtual source (in green), the panning gain is characterized by the length and colour of the large arrow, and also related to the intersection point between the directivity pattern and the green arrow.

Two observations arise from Figure 2. First, the main lobe of the directivity pattern is quite large regarding the angular spacing between loudspeakers. With a 2nd order encoding and decoding, one gets a thinner virtual directivity (2nd column of Figure 3, M=2) that helps making a more selective use of loudspeakers and creating more precise and robust sound images. With higher orders, even thinner directivities are involved instead, while requiring more loudspeakers in order to avoid "holes" between loudspeakers. The second comment is about the presence of non negligible secondary lobe(s). These are useful at low frequency for a proper reproduction of wave propagation properties (see also next section), but should be reduced regarding other criteria. This can be done by changing the proportion of the various elementary encoding patterns when combining them. In practice, this involves a modified decoding that consists in weighting ambisonic signals B_{mm}^{σ} by order-dependent gains g_m before applying the basic decoding matrix [16]. The so-called "max r_E" decoding [16] aims at "concentrating" the energy contributions towards the expected direction (see also in next section). As shown in Figure 3, it reduces secondary lobes without substantially enlarging the

main one. It is recommended for medium and high frequencies. The so-called "in-phase" [17] (or "controlled-opposite" according to Richard Furse's terminology) decoding completely removes secondary lobes, but enlarge quite significantly the main one. It is recommended for large listening area to limit the perception of loudspeakers in directions opposite to the expected one at off-centred listening positions.

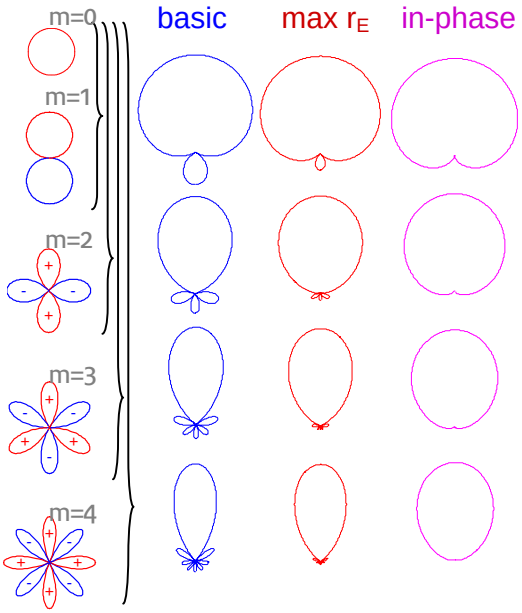

Figure 3 – Typical examples of recombination of encoding directivities (left column) of orders *m*=0 to 4, resulting in equivalent virtual microphone directivities, for three kinds of decoding. Getting from a virtual mic directivity to the next order's one, the lobes of the additional encoding pattern help (from front to rear) reinforcing the main lobe, thinning it, and reducing secondary lobes (while creating two others).

2.1.3. Characterization of spatial rendering

As explained just above, the distribution of the energy of signals emitted by loudspeakers gets confined in a thinner angular sector around the virtual source direction as higher order components are involved. As a consequence, the acoustic interference occurs mainly between waves from loudspeakers closer to each other, and therefore it gets larger. Finally, the wave front synthesized by wave interference is reconstructed over an area that extends as the order increases (Figure 4).

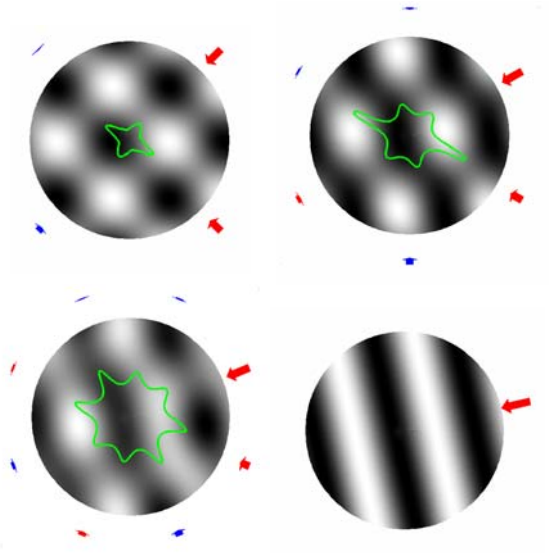

Figure 4 Progressive reconstruction of a wave front (right-bottom) with ambisonic encoding and decoding of orders *M*=1 to 3 (left to right, top to bottom), by interference of waves coming from resp. 2, 4, 6 loudspeakers (see conventions of Figure 2 for arrows).The boundary of well reconstructed area is shown as a constant-error contour.

So the area of well reconstructed sound field is bounded by the interference width. To get an idea of it, let's consider the case where the number *N* of loudspeakers fits the best the angular selectivity, *i.e.* *N*=2*M*+2. For some incidences, interference mainly occurs between waves with angular gap $2\pi/N=2\pi/(2M+2)$, and therefore its width is:

$$\Lambda(f)=\frac{c/f}{2\sin\left(\pi/(2M+2)\right)} \qquad (4)$$

Considering a centred listening area of radius *R*, and a "safety margin" R_m to avoid interference side effects, the sound field might be correctly rendered at the listener's ears up to a frequency $f_{\lim}$ such that $\Lambda(f_{\lim})=D=2(R+R_m)$. It has been numerically observed that the necessary safety margin decreases in inverse proportion to increasing order *M*, so that it can be approximately replaced by $R_m=R/M$:

$$f_{\lim}\approx\frac{cM}{4R(M+1)\sin\left(\pi/(2M+2)\right)}\approx\frac{cM}{2\pi R} \qquad (5)$$

A useful example is the case of a single, centred listener. Fixing R=8.8cm as a typical head radius, rounded values of f_{lim} are listed in Table 1 and used as reference in the analysis of microphone performances in section 6.

Above the frequency f_{lim}, a decoding that better "concentrates" the energetic contributions in the expected direction is recommended. That is the so-called "max r_E" decoding [16], which maximizes the norm r_E of the energy vector $\vec{E}$:

$$\vec{E} = \frac{\sum_{n=1}^{N} G_n^2 \vec{u}_n}{\sum_{n=1}^{N} G_n^2}, \text{ with } \vec{u}_n = \begin{pmatrix} \cos\theta_n \\ \sin\theta_n \end{pmatrix} \qquad (6)$$

where G_n is the signal gain associated to the loudspeaker n in the case of a single virtual source. In terms of perceived localisation, energy vector's norm r_E ($r_E \leq 1$) can be interpreted as a reduction factor of lateralisation effect [3]. That might result in an elevation effect of angle $\alpha_E = \text{acos}(r_E)$ when the listener turns the head. More generally, one could roughly consider that angle α_E characterizes the blur width of the created phantom image since in a particular, but representative case, the latter is produced by two loudspeakers at $+\alpha_E$ and $-\alpha_E$ around the virtual source direction. Values given in Table 1 are also used as reference in section 6. More generally $\alpha_E = \pi/(2M+2)$ for a M^{th} "max r_E" decoding.

Order M	1	2	3	4
f_{lim}	700 Hz	1300 Hz	1900 Hz	2500 Hz
α_E	45°	30°	22.5°	18°

Table 1 Limit frequencies f_{lim} of the acoustic reconstruction at a centred listener ears. Predicted angle α_E of the blur width of the phantom image.

2.2. Further acoustics basics for HOA

2.2.1. Fourier-Bessel series

HOA is grounded on spatial harmonic representation of 3D sound field, the so-called Fourier-Bessel series, which comes from the resolution of the homogeneous Helmholtz equation $(\Delta + k^2)\, p = 0$ (with wave number $k = 2\pi f / c$, frequency f and sound speed c) in a source-free region of space. In the spherical coordinate system shown in Figure 5 (radius r, azimuth θ, elevation δ), Fourier-Bessel series is defined as follow:

$$p(kr,\theta,\delta) = \sum_{m=0}^{\infty} i^m j_m(kr) \sum_{n=0}^{m} \sum_{\sigma=\pm 1} B_{mn}^{\sigma} Y_{mn}^{\sigma}(\theta,\delta) \qquad (7)$$

where

$$B_{mn}^{\sigma} = \frac{1}{i^m j_m(kr)} \iint_S p(r,\theta,\delta) Y_{mn}^{\sigma}(\theta,\delta)\, dS, \qquad (8)$$

if $j_m(kr) \neq 0$, S is the unit sphere.

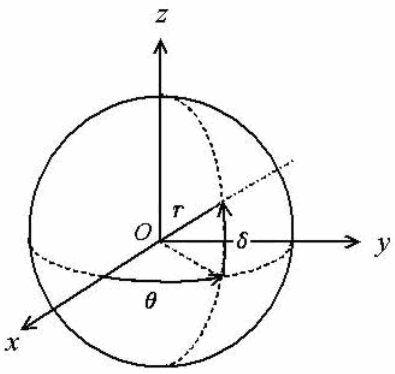

Figure 5 Spherical coordinate system in which any point of 3D Euclidean space is described by its radius r, its azimuth θ, and its elevation δ.

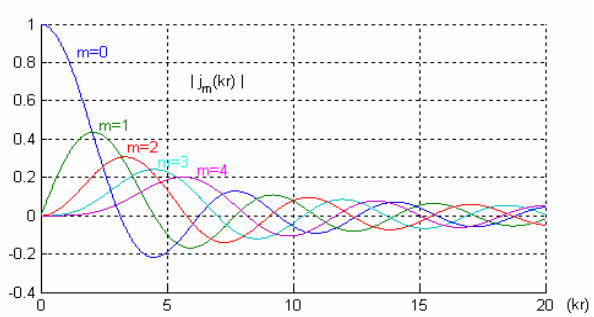

Figure 6 Illustration of spherical Bessel function up to order 4.

Radial[1] functions $j_m(kr)$ are spherical Bessel functions and are illustrated in Figure 6. Angular functions Y_{mn}^{σ} are the so-called spherical harmonics (Figure 7), with $m \geq 0$, $0 \leq n \leq m$ and $\sigma = \pm 1$. Various definitions of these functions exist and we use real spherical harmonics defined according to [18]:

[1] Note that the radial "distance" from origin actually depends on both radius and frequency.

$$Y_{mn}^{\sigma}(\theta,\delta)=\sqrt{(2m+1)(2-\delta_{0,n})\frac{(m-n)!}{(m+n)!}}P_{mn}(\sin\delta)\times\begin{cases}\cos n\theta & \text{if } \sigma=+1\\ \sin n\theta & \text{if } \sigma=-1\end{cases}\quad(\text{ignored if } n=0) \tag{9}$$

where $P_{mn}(\sin\delta)$ are the associated Legendre functions.

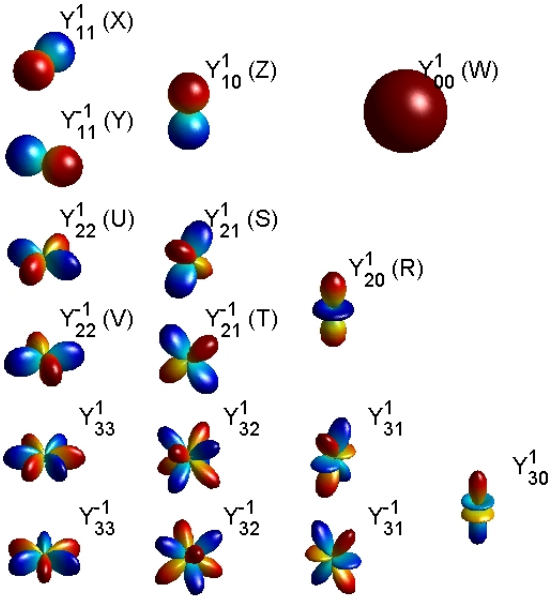

Figure 7 3D view of spherical harmonics up to order 3 with usual designation of associated HOA components.

The case of a sound field consisting of a plane wave is of particular interest. Considering a wave incidence (θ_S, δ_S) and a conveyed signal S leads to the following expression of ambisonic components:

$$B_{mn}^{\sigma}=S.Y_{mn}^{\sigma}(\theta_S,\delta_S) \tag{10}$$

This equation provides new, 3D encoding laws that complete equations (1) or can be used instead. They yield $(M+1)^2$ components for an M^{th} order 3D representation. The spatial decoding process is very similar as in 2.1.2, but requires "periphonic" (3D) loudspeaker setups (e.g. according to polyhedral geometries). For further explanation, refer to [3].

2.2.2. HOA representation and sound field approximation

The M-order truncation of Fourier-Bessel series provides an approximate representation of the sound field:

$$p_M(kr,\theta,\delta)=\sum_{m=0}^{M}i^m j_m(kr)\sum_{n=0}^{m}\sum_{\sigma=\pm1}B_{mn}^{\sigma}Y_{mn}^{\sigma}(\theta,\delta) \tag{11}$$

This approximation requires $K=(M+1)^2$ HOA signals. In order to objectively characterize the approximation accuracy, we use the Normalized Mean Square Error (NMSE) associated to a finite order of truncation M:

$$e(kr)=\frac{\iint_S|p(kr,\theta,\delta)-p_M(kr,\theta,\delta)|^2\,dS}{\iint_S|p(kr,\theta,\delta)|^2\,dS}, \tag{12}$$

where S is the unit sphere. For the particular case of a sound field only made by plane waves, Equation (12) can be simplified [19]:

$$e(kr)=1-\sum_{m=0}^{M}(2m+1)\left(j_m(kr)\right)^2 \tag{13}$$

In this case, the error $e(kr)$ is independent of angular position of the source. Figure 8 illustrates the NMSE as a function of kr for truncation orders going from 0 to 15.

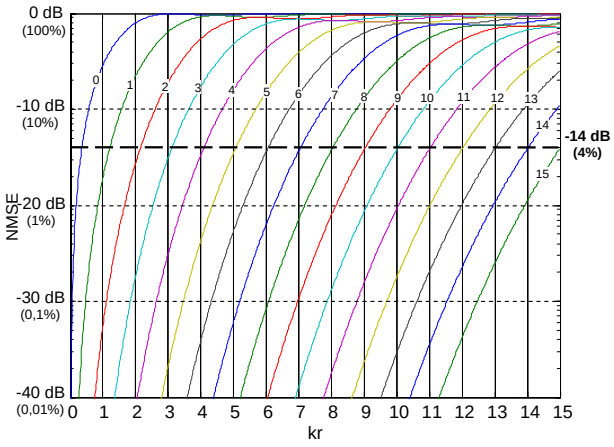

Figure 8 Normalized Mean Square Error for the plane wave case and order 0 to 15.

Clearly, it shows that for a constant value of error (e.g. 4% represented by the dotted line in Figure 8), i.e. for the same approximation accuracy, the higher kr, the higher the truncation order M should be. Moreover, the dotted line in Figure 8 corresponding to a 4% error cut

the curves such that $M = kr$ approximately. Thus, for a given wave number K (or a corresponding frequency) and a given radius R of the approximation sphere, a simple rule can defined to determine the order that allow a reasonably accurate approximation of the sound field [19]:

$$M = \lceil KR \rceil, \qquad (14)$$

where $\lceil \cdot \rceil$ denotes rounding up to the nearest integer. For example if we wish to represent a 1kHz plane-wave field within a sphere of radius 0.1m with a 4% error, this rule indicates a sufficient truncation order of value 2. But for a 5kHz plane-field within the same sphere of radius 0.1m and with 4% error, the truncation order must be at least equal to 9.

It's worth noticing that equation (11) fully complies with estimation of frequency limit given by (5). Such considerations can provide a criterion for the design of HOA microphone system and for the assessment of its performance in term of potential spatial rendering (see section 6.3).

3. THEORETICAL BASES OF SPHERICAL MICROPHONE FOR HOA RECORDING

Direct recording of HOA signals that describe an actual sound field using of directional microphones located at one single point is not feasible. An alternative method consists in deriving HOA signals from a set of acoustic measurements made by usual microphones and a corresponding mathematical model which relates these quantities to HOA signals. In this section, we first study continuous modeling of the problem of HOA signals estimation. Then, we transpose the continuous models into their discrete counterparts and discuss induced spatial aliasing.

3.1. Mathematical modeling of a continuous spherical HOA microphone

3.1.1. Spherical microphone derived from spherical Fourier transform

The spherical Fourier transform (8) suggests a theoretical method of estimating HOA signals from the recording of acoustic pressure over a continuous spherical surface of radius *R*. This method illustrated in Figure 9 consists in projecting the continuous spherical measurement onto the spherical harmonic basis and equalizing the resulting signals according to their order by means of filters $EQ_m(kR) = 1/i^m j_m(kR)$. Nevertheless, this method is valid only if $j_m(kR) \neq 0$. Unfortunately, the Figure 6 shows that for all m orders, $j_m(kR)$ takes the zero value regularly over the kr range. Moreover, when $EQ_m(kR)$ is defined, it yields a huge signals amplification for *kR* around the zeros of $j_m(kR)$. Such amplification is impracticable.

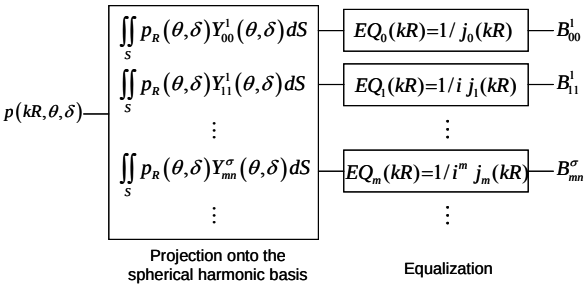

Figure 9 Schematic view of a theoretical spherical HOA microphone.

The huge amplification reflects difficulties encountered by the spherical microphone to estimate HOA signals from measures. These difficulties are partly explained by the lack of intrinsic directivity of the spherical microphone. Indeed, only phase differences exist between each measurement point in order to distinguish all spherical harmonics components. This creates indeterminate frequencies that are functions of the radius and the order, and correspond to the zeros of the spherical Bessel functions. For example, the zero order HOA signal B_{00}^1 in the Fourier Bessel series can't be estimated with a spherical sensor array at frequencies $f_a = a\,c/2R$, where a is a positive integer, c the celerity of sound, and R the radius of the sphere, that is at wave numbers $k = 2R$. A solution to avoid undetermined frequencies is to make the sensors measurements directional.

3.1.2. Improving the spherical microphone directivity

Usual directional sensors can be used to improve the microphone directivity. A 1st order directional sensor records a signal proportional to a combination of acoustic pressure and particle velocity:

$$s(kR,\theta,\delta) = \alpha\, p(kR,\theta,\delta) + (1-\alpha)\rho c \frac{\partial p(kR,\theta,\delta)}{\partial kR} \qquad (15)$$

where ρc characterizes acoustic impedance. Typically $0 \le \alpha \le 1$ in order to obtain the maximum value 1 at the

incidence ($\theta = 0^\circ, \delta = 0^\circ$). By introducing Equation (15) in the Fourier Bessel series (7), we obtain the spherical harmonic expansion of a 1st order directional measure:

$$s(kR,\theta,\delta) = \sum_{m=0}^{\infty} i^m \left(\alpha\, j_m(kR) - (1-\alpha)\, j'_m(kR)\right) \times \sum_{n=0}^{m} \sum_{\sigma=\pm 1} B_{mn}^{\sigma}\, Y_{mn}^{\sigma}(\theta,\delta) \tag{16}$$

where $j'_m(kR)$ is the first derivative of $j_m(kR)$ according to kR. Orthogonal projection of $s(kr,\theta,\delta)$ onto the spherical harmonic basis leads to the following expression of HOA signals:

$$B_{mn}^{\sigma} = \frac{1}{i^m \left(\alpha j_m(kR) - (1-\alpha) j'_m(kR)\right)} \times \iint_S s(kR,\theta,\delta) Y_{mn}^{\sigma} dS \tag{17}$$

allowing us to deduce HOA signals in a similar way as shown in Figure 9, the equalization process being defined as follow:

$$EQ_m(kR) = \frac{1}{\left(\alpha\, j_m(kR) - (1-\alpha)\, j'_m(kR)\right)}$$

With $\alpha\, j_m(kR) - (1-\alpha)\, j'_m(kR) \neq 0$. This radial expression is illustrated in Figure 10 for the particular case of cardioid sensors, i.e. for $\alpha = 0{,}5$. The figure shows that this function equals the zero value only for $kR = 0$ (and orders $m \geq 1$), and then seems to be more adapted to HOA signal recording over a large frequency band.

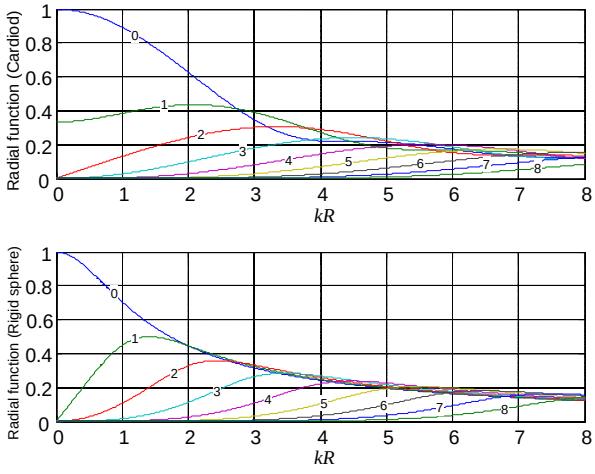

Figure 10 Radial functions for directional HOA microphone: cardiod sensors (top) and omnidirectional sensors at the surface of a rigid sphere (bottom).

A different approach for improving the directivity of continuous spherical microphone consists in introducing into the sound field a diffracting structure, e.g. a rigid sphere. Such a rigid sphere has already been used by Gary Elko [20] for the construction of a 1st order differential microphone with 3D adjustable orientation and more recently for spatial sound recording and beamforming [9, 21] in parallel to authors' work. In presence of a rigid sphere, the sound field is defined as a combination of direct and diffracted sound pressure [18]:

$$p_{\text{rig}}(kr,\theta,\delta) = \sum_{m=0}^{+\infty} \left(j_m(kr) - \frac{j'_m(kR)}{h_m^{-\prime}(kR)} h_m^{-}(kr) \right) \times \sum_{n=0}^{m} \sum_{\sigma=\pm 1} B_{mn}^{\sigma}\, Y_{mn}^{\sigma}(\theta,\delta) \tag{18}$$

where R is the radius of the sphere, $h_m^{-}(kr)$ the divergent Hankel function, and $h_m^{-\prime}(kR)$ its 1st derivative according to kR. A particularly interesting case is the recording of acoustic pressure at the surface of the rigid sphere ($r = R$):

$$p_{\text{rig}}(kR,\theta,\delta) = \sum_{m=0}^{+\infty} \left(\frac{i^{m-1}}{(kR)^2\, h_m^{-\prime}(kR)} \right) \times \sum_{n=0}^{m} \sum_{\sigma=\pm 1} B_{mn}^{\sigma}\, Y_{mn}^{\sigma}(\theta,\delta) \tag{19}$$

The radial dependence between brackets is shown in Figure 10. As for the cardioid sensor case, this radial function equals zero only for $kr = 0$ (and $m > 0$). Orthogonal projection of Equation (19) onto the spherical harmonic basis leads to the following expression of HOA signals:

$$B_{mn}^{\sigma} = \left(i^{-m+1} (kR)^2\, h_m^{-\prime}(kR) \right) \times \iint_S p_{\text{rig}}(kR,\theta,\delta) Y_{mn}^{\sigma}(\theta,\delta)\, dS \tag{20}$$

which is defined for $i^{-m+1}(kR)^2\, h_m^{-\prime}(kR) \neq 0$, i.e. for $m > 0$ and $kR > 0$ as we can see in (Figure 4). HOA signal can therefore be estimated according to the method describe in Figure 9 by defining equalisation filters as follow: $EQ_m(kR) = i^{-m+1}(kR)^2\, h_m^{-\prime}(kR)$.

In conclusion, directional spherical microphone seem to be more adapted than omnidirectional one to HOA recording since equalisation filters are defined for all non-null frequencies. Nevertheless, we can see in Figure 10 that an excessive amplification remains below a limit value of kR that increases with order m. Indeed,

especially for higher orders and low frequencies, the microphone tries to catch spatial information that is very poor at the measurement point and is substantial only at a distance from the recording system. Consequently, the microphone will be in this case very sensitive to estimation errors (*e.g.* sensor self-noise, position errors).

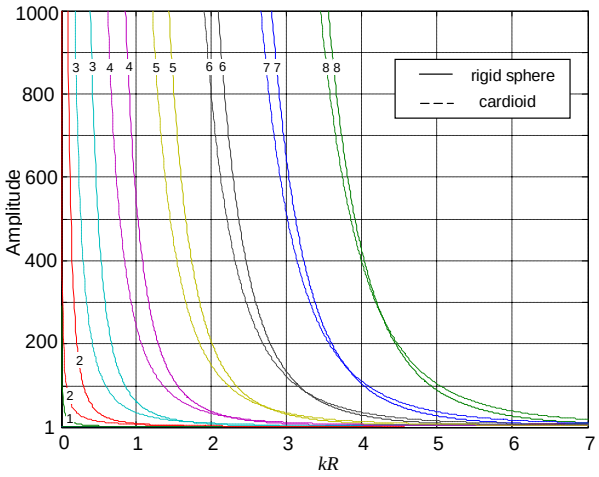

Figure 11 Inverse of radial functions $\left|EQ_m(kR)\right|$ for cardioid and rigid sphere cases.

3.2. Discretization of the continuous spherical microphone

3.2.1. Discrete formulation of the estimation problem

In order to realize a spherical HOA microphone, we must use a finite number of sensors. On a spherical surface of radius R, we define a set of Q points at locations given by the angles (θ_q, δ_q), $1 \le q \le Q$. We only take into account the cases of spherical directional microphone and omnidirectional sensors at the surface of a rigid sphere. In these two cases, the q[th] sensor picks up an acoustic signal which can be expressed as follow:

$$S_q = \sum_{m=0}^{+\infty} W_m(kR) \sum_{n=0}^{m} \sum_{\sigma=\pm 1} B_{mn}^{\sigma} Y_{mn}^{\sigma}(\theta_q, \delta_q) \qquad (21)$$

where

$$W_m(kR) = \begin{cases} \alpha\, j_m(kR) + i(\alpha - 1)\, j_m'(kR) \\ \text{directional microphones} \\ \\ i^{-m+1} (kR)^2 \, h_m'(kR) \\ \text{rigid sphere} \end{cases} \qquad (22)$$

Actually, we can estimate HOA signals up to a restricted order M such that the total number $K=(M+1)^2$ of components does not exceed the number Q of sensors ($K \le Q$). Thus, we consider the M order truncation of Equation (21). The resulting system of linear equations can be written in discrete matrix form:

$$\mathbf{T} \cdot \mathbf{b} = \mathbf{s}, \qquad (23)$$

where the $Q \times K$ "transfer matrix" $\mathbf{T}$, the K-length column vector $\mathbf{b}$ and the Q-length column vector $\mathbf{s}$ are defined as follow, respectively:

$$\mathbf{T} = \begin{pmatrix} Y_{00}^1(\theta_1, \delta_1) & \cdots & Y_{M0}^1(\theta_1, \delta_1) \\ \vdots & \vdots & \vdots \\ Y_{00}^1(\theta_Q, \delta_Q) & \cdots & Y_{M0}^1(\theta_Q, \delta_Q) \end{pmatrix} \cdot \mathrm{diag}[W_m(kR)]$$

$$= \mathbf{Y} \cdot \mathrm{diag}[W_m(kR)], \quad 0 \le m \le M$$

$$\mathbf{s} = \left(S_1, S_2, \ldots, S_Q\right)^t, \; \mathbf{b} = \left(B_{00}^1, B_{11}^1, B_{11}^{-1}, B_{10}^1, \ldots, B_{M0}^1\right)^t.$$

Due to the spherical geometry of the microphone array, the matrix $\mathbf{T}$ is a product of a real matrix $\mathbf{Y}$ whose columns are sampled spherical harmonics $\mathbf{y}_{mn}^{\sigma}$ by a diagonal matrix of radial-dependent filters. The vector $\mathbf{s}$ contains the signals recorded by the Q sensors and $\mathbf{b}$ is the vector whose elements are the unknown HOA signals up to a finite order M. These two last vectors are connected by a discrete mathematical model, the matrix $\mathbf{T}$.

3.2.2. "Naive" least-squares resolution and instability of the solution

Since the matrix $\mathbf{T}$ is a $Q \times K$ rectangular matrix with more rows than columns ($Q \ge K$), the system (23) is overdetermined. In general, such a linear system cannot be solved exactly and the problem amounts to find an approximate solution which minimizes the square norm of the residual [22]:

$$\min_{\mathbf{b}} \left\| \mathbf{s} - \mathbf{T}\mathbf{b} \right\|_2^2.$$

The solution $\mathbf{b}_{LS}$ to this minimization problem satisfies a new system of linear equations called normal equations [22]:

$$(\mathbf{T}^* \mathbf{T})\mathbf{b}_{LS} = \mathbf{T}^* \mathbf{s}. \quad (24)$$

where $\mathbf{T}^*$ denotes the transpose conjugate of the complex matrix $\mathbf{T}$. As the columns of the matrix $\mathbf{T}$ are linearly independent, the definite positive matrix $\mathbf{T}^*\mathbf{T}$ is invertible and the solution of the system (24) can be expressed as follow [22]:

$$\mathbf{b}_{LS} = \left(\mathbf{T}^* \mathbf{T}\right)^{-1} \mathbf{T}^* \mathbf{s}. \quad (25)$$

$\mathbf{b}_{LS}$ is the least-squares solution of the system (23), i.e. the solution which corresponds to projecting $\mathbf{b}$ onto the columns space of $\mathbf{T}$. By introducing the factorized expression of the matrix $\mathbf{T}$ in Equation (25), we finally obtain:

$$\mathbf{b}_{LS} = \mathrm{diag}\left[\frac{1}{W_m(kR)}\right]\mathbf{E}\,\mathbf{s}, \quad (26)$$

where

$$\mathbf{E} = \left(\mathbf{Y}^t \mathbf{Y}\right)^{-1} \mathbf{Y}^t.$$

The real matrix $\mathbf{E}$ is usually called the Moore-Penrose inverse of the matrix $\mathbf{Y}$ [22].

The "naïve" least-squares resolution of the system (23) provides an easy way to compute its best approximate solution $\mathbf{b}_{LS}$ in the least-squares sense. Nevertheless, even if the residual is theoretically minimized, the solution becomes meaningless when $W_m(kR)$ is very small, i.e. corresponding to low frequencies and highest estimate order. Indeed, the system (24) is in this case particularly instable so that small errors in the measure vector $\mathbf{s}$, e.g. due to sensor self-noise or sensor position errors, are magnified in the resulting estimation of HOA signals $\mathbf{b}_{LS}$. A useful objective indicator of non-stability of the system (24) is the condition number of the matrix $(\mathbf{T}^* \mathbf{T})$ defined by [22]:

$$\kappa(\mathbf{T}^*\mathbf{T}) = \left\|\mathbf{T}^*\mathbf{T}\right\|_2 \left\|\left(\mathbf{T}^*\mathbf{T}\right)^{-1}\right\|_2. \quad (27)$$

The ideal condition number is worth 1 and means that all columns in the matrix are linearly independent and of balanced norm. When the level difference between columns vectors become too large, $\kappa(\mathbf{T}^*\mathbf{T})$ increases. The matrix $\mathbf{T}^*\mathbf{T}$ is said ill-conditioned if $\kappa(\mathbf{T}^*\mathbf{T})>>1$. The resulting relative error of the least squares solution can be as large as the product of the relative residual by the condition number [22]:

$$\frac{\left\|\mathbf{b}-\mathbf{b}_{LS}\right\|_2}{\left\|\mathbf{b}_{LS}\right\|_2} \le \kappa(\mathbf{T}^*\mathbf{T}) \frac{\left\|\mathbf{T}^*\mathbf{s}-\mathbf{T}^*\mathbf{T}\mathbf{b}_{LS}\right\|_2}{\left\|\mathbf{T}^*\mathbf{s}\right\|_2}. \quad (28)$$

Consequently, a poorly conditioned matrix $\mathbf{T}$ can lead to a physically meaningless solution. Hence, this solution must be replaced by an approximated one where the noisy components are filtered out (cf. Section 4.1).

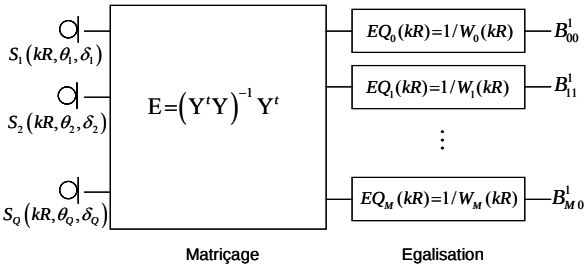

Figure 12 Discrete spherical HOA microphone processing.

3.2.3. Limitations introduced by discretization: spatial aliasing

The discrete formulation of the problem of HOA recording introduces some limitations in the estimation process. These limitations concern first the frequency band of HOA signals: according to the so-called Shannon criterion, the larger distance d between sensors defines a limit frequency above which spatial aliasing occurs:

$$f_{\mathrm{al}} = \frac{c}{2d} = \frac{c}{2R\gamma}, \quad (29)$$

where c is the sound speed, R is the radius of the microphone array, and γ is the maximum angle between two sensors.

Furthermore, spatial aliasing also concerns undersampled spherical harmonic functions. The number of distinguishable harmonics by the microphone array depends on both the number of sensors and their positions on the sphere. For example, in order to estimate K different spatial harmonics up to a maximal order M, at least K sensors are needed to sample them correctly. Moreover, the sensor positions must satisfy the discrete orthonormality properties for sampled spherical harmonics:

$$\frac{1}{Q}\mathbf{y}_{mn}^{\sigma\ t} \cdot \mathbf{y}_{m'n'}^{\sigma'} = \delta_{mm'}\delta_{nn'}\delta_{\sigma\sigma'}, \quad (30)$$

where $0 \le m, m' \le M$, $0 \le n, n' \le m$, $\sigma, \sigma' = \pm 1$, and the Kronecker delta δ_{ij} equals 1 if $i = j$ and 0 otherwise. Finally, spatial aliasing due to higher order harmonics must be taken into account. Indeed, when undersampled spherical harmonics of higher order than M are present in the sound field, they fold up on the lower components and can severely corrupt the estimation of HOA signals. To suitably minimize spatial aliasing effects, the sensors placed on the sphere must be in general more numerous than the HOA signals that we seek to estimate, i.e. $Q > K$ in the system (23).

4. PRACTICAL DESIGN OF SPHERICAL HOA MICROPHONE

This section aims at deriving a meaningful solution to HOA signal estimation by choosing a suitable sampling scheme on the sphere and introducing a regularization process based on Tikhonov filters [23].

4.1. Practical equalization involving regularization filters

4.1.1. Filtering approach of regularization

The regularization process aims at damping the noisy frequency components of HOA signals resulting from the least-squares resolution of the system (24). As explained above, this filtering concerns essentially low frequency bands of HOA signals of highest orders. As we assume that the sampled spherical harmonic matrix $\mathbf{Y}$ is near to be orthonormal, the regularization can be realized by introducing a filter in the equalization:

$$\mathbf{b}_{REG} = diag\left[F_m(kR) \cdot \frac{1}{W_m(kR)} \right] \mathbf{E}\,\mathbf{s} \qquad (31)$$

where $F_m(kR)$ is the regularization filter, and the vector $\mathbf{b}_{REG}$ contain the regularized HOA signals. An optimal regularization filter $F_m(kR)$ suppresses noise in the data vector $\mathbf{s}$ while keeping at the same time all relevant information. Various definition of the filter coefficients can be obtained by imposing additionally constraints on the least-square problem (24). The most commonly used method of regularization is probably the Tikhonov method [23]. Standard form of Tikhonov regularization imposes a maximal energy for the solution, *i.e.* resulting HOA signals. This method can be interpreted by defining the filters as:

$$F_m(kR) = \frac{\left|W_m(kR)\right|^2}{\left|W_m(kR)\right|^2 + \lambda^2}. \qquad (32)$$

λ is the regularization parameter. For λ equals to 0, $F_m(kR) = 1$ and b_{REG} simply correspond to HOA signals obtained by the direct least squares resolution of the system. As λ increases, $F_m(kR)$ decay to zero, implying that an λ too large will result in over regularized solution. Note that filters $F_m(kR)$ are proportional to $\left|W_m(kR)\right|^2$ and therefore they decay fast enough to compensate for the increasing factor $1/W_m(kR)$. Figure 13 shows $F_m(kR)$ as a function of $\left|W_m(kR)\right|$. Note that Tikhonov filters (cont. line) can be interpreted as a 1st order approximation of an exponential attenuation (dashed line). Equalization filters are finally defined by:

$$EQ_m(kR) = \frac{\bar{W}_m(kR)}{\left|W_m(kR)\right|^2 + \lambda^2}, \qquad (33)$$

where $\bar{W}_m(kR)$ is the complex conjugate of $W_m(kR)$. We can recognise the standard expression of Tikhonov regularization used for instable filters [24].

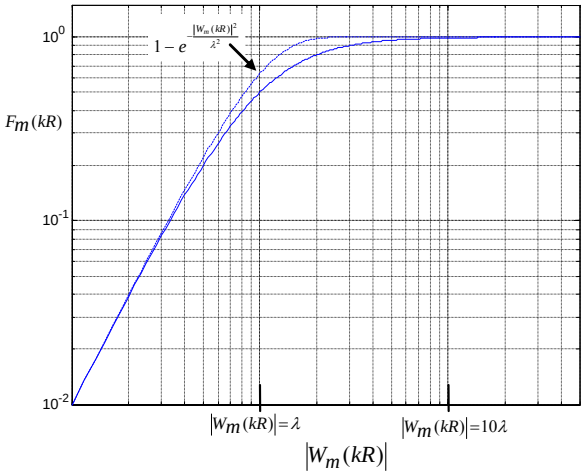

Figure 13 Illustration of the regularization filter $F_m(kR)$ as a function of $\left|W_m(kR)\right|$.

4.1.2. Choice of the regularization parameter

A suitable choice of regularization parameter λ is not trivial. Indeed, too large values of λ yield over-filtered solution. On the other hand, a too small parameter results in not enough filtered one. An ideal parameter must avoid noise in the solution while preserving at the

same time all of its relevant information. The regularization parameter λ can be related to a unique maximal amplification factor a induced by the filters $F_m(kR)$:

$$\lambda = \frac{1-\sqrt{1-1/a^2}}{1+\sqrt{1-1/a^2}}. \quad (34)$$

The choice of the maximal amplification factor a can advantageously take into account improvement in the signal to noise ratio due to the use of multiple sensors. In this case, a is directly connected to sensor noise amplification by:

$$a = \sqrt{Q}\,10^{\frac{a_s}{20}}.$$

where a_s is the maximum sensor noise amplification expressed in dB, and Q is the total number of sensors used. A large number of sensors improves the signal to noise ratio of the spherical microphone array and yield to a larger amplification factor a (for a constant maximal noise amplification a_s), and so an accurate estimation of HOA signals. In general, the regularization parameter λ can be set by trial and error method.

4.2. Spatial sampling on the sphere

4.2.1. Equiangular sampling

In a way similar to the standard sampling theorem in one dimensional space, Driscoll and Healy [25] stated that a band limited function defined on a sphere, *i.e.* a function for which $B_{mn}^{\sigma}=0$ if $m>M$ can be exactly recovered from a finite sum of samples of this function. This requires to sample uniformly and independently the angles θ and δ at $2M+2$ locations:

$$\begin{aligned} \theta_i &= \frac{\pi i}{2M+2}, \quad i = 0,\ldots,2M+1 \\ \delta_j &= \frac{2\pi j}{2M+2} \quad j = 0,\ldots,2M+1 \end{aligned} \quad (35)$$

Exact formulation of HOA signals up to order M is then expressed as follow:

$$B_{mn}^{\sigma} = \frac{1}{W_m(kR)}\,\frac{\sqrt{2\pi}}{2M+2}\sum_{i=0}^{2M+1}\sum_{j=0}^{2M+1}\alpha_i\, s_R(\theta_i,\delta_j)\,Y_{mn}^{\sigma}(\theta_i,\delta_j) \quad (36)$$

where the coefficients α_i given in [25] have been introduced to compensate for the difference between the density of points near the poles and that in the equatorial zone. Equation (36) requires $4(M+1)^2$ sensors arranged on the sphere to compute HOA signals up to M order.

It is however possible to reduce by half this number by using a Gaussian quadrature [26]. δ is then sampled at unequally spaced angles according to the $M+1$ zeros of Legendre polynomials, so that $P_{M+1}(\sin\delta_j)=0$, $j=0,\ldots,M$. Equation (36) becomes:

$$B_{mn}^{\sigma} = \frac{1}{W_m(kR)}\sum_{i=0}^{M+1}\sum_{j=0}^{2M+1}\alpha_j\, s_R(\theta_i,\delta_j)\,Y_{mn}^{\sigma}(\theta_i,\delta_j) \quad (37)$$

where the coefficients α_j are the associated weights to Gauss sampling [26]. Nevertheless, the total number $2(M+1)^2$ of sensors required remains very high and not optimal. In order to reduce this number, we need to find more regular sampling schemes.

4.2.2. Regular and semi-regular polyhedral sampling

Unfortunately, it is not possible to uniformly sample the surface of a sphere, except in five particular cases, according to the vertices of Plato's polyhedrons [27]: tetrahedron, hexahedron, octahedron, dodecahedron and icosahedron. As these regular point distributions are not defined directly according to spherical harmonics, we need to examine the orthonormality properties of induced sampled spherical harmonics. This can be done by considering the orthonormality error matrix defined by:

$$\mathbf{D} = \mathbf{I}_K - \frac{1}{Q}\mathbf{Y}^t\cdot\mathbf{Y}, \quad (38)$$

where I_{K_2} is the $K\times K$ identity matrix with $K=(M+1)^2$, Q is the number of sampling points, and the columns of the matrix Y are sampled spherical harmonics. Figure 14 shows the matrix **D** associated to all five regular polyhedrons. Orthonormality error between two sampled spherical harmonics is represented by a small gray square. For more clarity, harmonics of different orders are separated by lines. We can see that the tetrahedron, the hexahedron, and the dodecahedron yield arrangements which satisfy exactly the orthonormality condition up to order 1. Note that the so-called SoundField microphone [5] used for Ambisonics recording (1st order HOA) is based on a tetrahedral sampling scheme. The icosahedron and the dodecahedron vertices preserve the orthonormality properties of sampled spherical harmonics up to order 2.

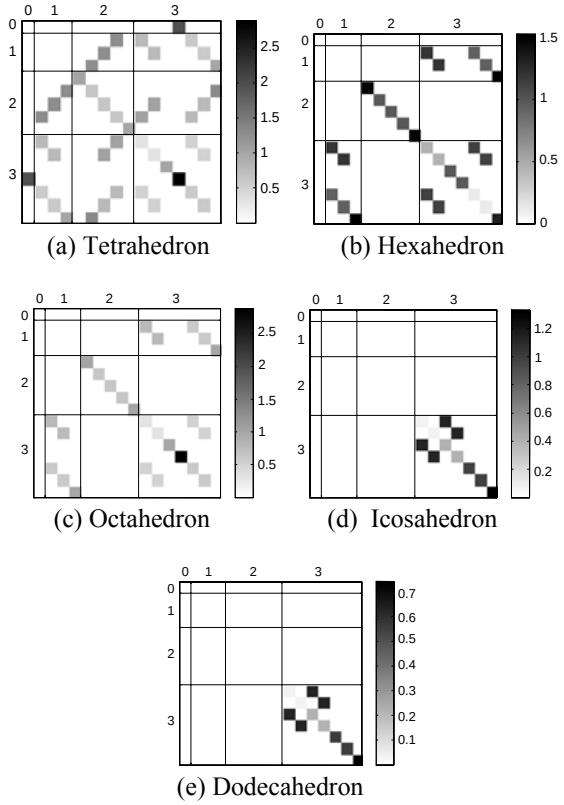

Figure 14 Matrices of orthonormality error for the five regular polyhedrons. Gray level is related to error level.

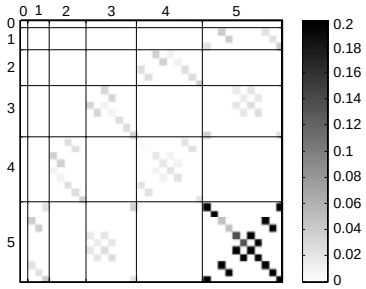

Figure 15 Matrix of orthonormality error associated to the pentakis-dodecahedron. Gray level is related to error level.

In order to record higher order HOA signals, sampling schemes based on semi-regular polyhedrons, *i.e.* convex polyhedrons for which faces are regular polygons but at least of two different types, can be investigated. We have constructed a 4th order spherical microphone based on the vertices of a pentakis-dodecahedron which consists of a combination of an icosahedron and a Dodecahedron (cf. Figure 16). The matrix of orthonormality error of such a polyhedron is represented in Figure 15 and will be discussed in Section 5.

4.2.3. Quasi-uniform sampling

Now the question is: how to arrange in a homogeneous way a set of points at the surface of a sphere? The answer depends on the mathematical definition of "homogeneous" that we choose. Indeed, different existing interpretations lead to slightly different arrangements. For example, a first approach consists in finding the centres of non-overlapping identical circles such that their radius is maximized (packing problem). Another very similar method aims at defining the centres of overlapping identical circles which entirely cover the surface of the sphere such that their radius is minimized (covering problem). A last example to define point positions on a sphere derives from solving the problem of finding the lowest energy configuration of point charges on a conducting sphere (Thomson problem). Results of all these methods are available on Internet for various numbers of points, e.g. [28, 29]. Although these methods yield a relative equidistance between sensors, they are not directly linked to spherical harmonics and don't guarantee the orthonormality condition for sampled spherical harmonics. The properties must be analyzed in terms of the orthonormality error matrix **D** define by Equation (38).

5. CONSTRUCTION OF A 4TH ORDER PROTOTYPE

5.1. Geometrical description and associated characteristics

5.1.1. The choice of sensor positions

The distribution of sensors on the rigid sphere is based on the 32 vertices of a pentakis-dodecahedron shown in Figure 16. Such a polyhedron can be seen as the association of a dodecahedron (12 vertices) and an icosahedron (20 vertices). This sampling scheme is not exactly uniform since angles between sensors are not equal. Indeed, angular gap between two vertices of the dodecahedron and between one vertex of the dodecahedron and one of the icosahedron are worth 0.73 and 0.65 radians, respectively. Nevertheless, as we can see in Figure 15 the discrete spherical harmonics associated to this sampling scheme is very close to be

orthonormal up to order 4 although the maximum diagonal term and the maximum off-diagonal term correspond to an error of 3.7% and 3.73%, respectively. Also, we can see in Figure 15 that spatial aliasing could potentially occur in the 1st and 3rd orders if the 5th order is strongly present in the sound field near the sensors.

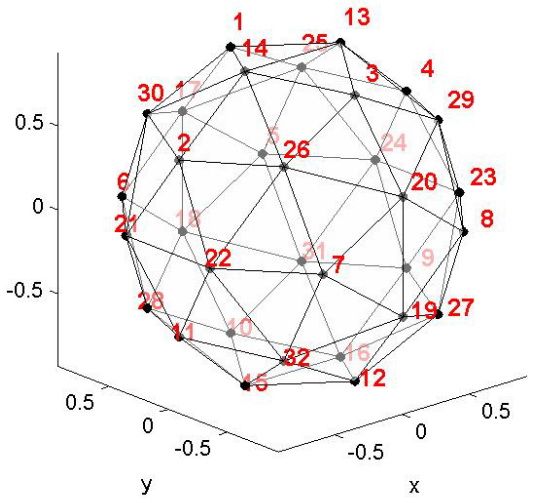

Figure 16 Spherical distribution of sensors according to the 32 vertices of a pentaki-dodecahedron.

5.1.2. The choice of the radius

The choice of the radius results from a compromise between spatial aliasing at high frequencies and consistence of estimation at low frequencies for highest order. The radius of our prototype is worth R=3,5cm which corresponds to approximates aliasing frequencies of 6700Hz and 7500Hz for the largest angular gap and the smallest one, respectively. The size of the spherical microphone array also determines the "presence level" of HOA signals according to order by means of the functions $W_m(kR)$. Since the sampled spherical harmonic matrix $\mathbf{Y}$ is approximately orthonormal, the condition number of the matrix $\mathbf{T}^*\mathbf{T}$ in Equation (24), *i.e.* the stability of the estimation process, depends only on the functions $W_m(kR)$ (and so the radius R):

$$\kappa(\mathbf{T}^*\mathbf{T}) = \frac{\max(|W_m(kR)|^2, m=0\ldots M)}{\min(|W_m(kR)|^2, m=0\ldots M)} \qquad (39)$$

Figure 17 illustrates the modulus of the functions $W_m(kR)$ for orders m=0 to 4 in parallel to the condition number of the matrix $\mathbf{T}^*\mathbf{T}$. We can easily see that $\kappa(\mathbf{T}^*\mathbf{T})$ rapidly increases while the difference between $W_m(kR)$ of distinct orders increases. Instability occurs in highest orders and at low frequencies.

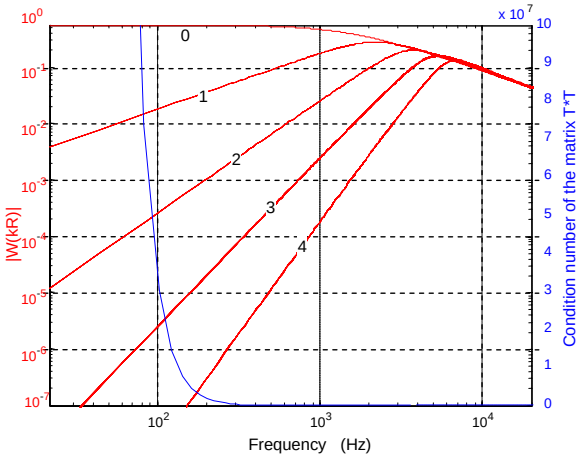

Figure 17 Functions $|W_m(kR)|$ and the condition number of the transfer matrix $\mathbf{T}^*\mathbf{T}$ as a function of frequency (r=3,5cm).

5.2. Realization and implementation of the prototype

The 4th order HOA microphone prototype illustrated in Figure 18 is made of an empty plastic ball that is acoustically non-strictly rigid. Holes are distributed over the sphere to incorporate a regular configuration of HOA microphone network. Small placement errors may occur and could be corrected with post signal processing. The sphere is cut into two parts to insert the 32 sensors from inside. The sensors wires are pool together to a plastic sheath fixed to the ball. Sensors close to the sheath will have directivity errors compared to theoretical model discussed in 6.3.

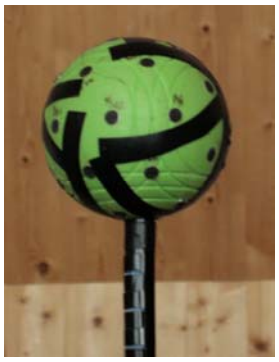

Figure 18 32 sensors compose the 4th order HOA microphone prototype.

Figure 19 shows regularization filters associated to the prototype for different maximal sensor noise amplification: 0dB, 6dB and 20dB.

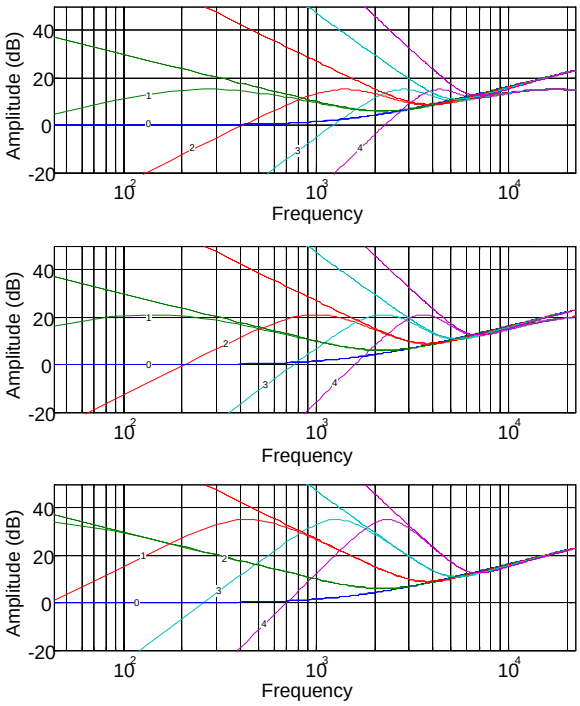

Figure 19 Amplitude of theoretical and regularized equalization filters $EQ_m(kR)$ (dashed lines and cont. lines resp.) with 3 different regularization parameters corresponding to 3 max. *noise amplification* levels: 0dB, 6dB, and 20dB. (Note that maximal gains of equalization filters go +15dB beyond these limit values, accordingly to the number of sensors used.)

Acquisition system is composed of a 32 channel home-made preamplifier, two MOTU 24I/O AD converters plugged to a MOTU PCI424 card in a computer. The software Plogue Bidule is used in combination with VST plug-ins to make real-time recording and rendering over a predefined configuration of loudspeakers or over headphones.

6. OBJECTIVE MEASUREMENTS AND VALIDATION

6.1. Measurements

6.1.1. Free field measurements

The 4th order, 32 sensor prototype microphone has been measured in IRCAM anechoic chamber. It has been mounted on a Brüel and Kjær turn table situated in the middle of the room allowing azimuth rotation. Two laser lights installed above the system and at 0° elevation respectively indicate the centre position of the microphone. A Tannoy loudspeaker mounted on a moving arm allowing elevation measurements was used. The setup is shown Figure 20.

The spherical microphone array has been measured every 5 degrees from 0 to 360 degrees azimuth and from -40 to 90 degrees elevation, totalizing N=1971 measures for each microphone. The correlation between the 0 degree and the 360 degrees azimuth sensors response has been calculated verifying the measures repeatability.

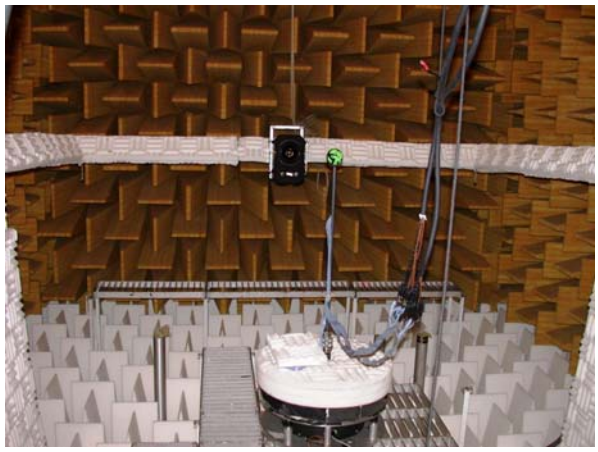

Figure 20 Free field measurements setup for the 32 sensors microphone in IRCAM anechoic chamber.

A Studer 24 channel preamplifier has been used for the acquisition measurements. Therefore measurement procedure has been performed twice to get the responses of 24 sensors at once. 12 sensors have been measured twice allowing us to verify the measures.

We used logarithm sine sweep method with a 16th order sequence. We placed the signal level in order to have at least 30dB dynamic range to the measured impulse response.

During the measurements it was not sure that the centre of the sphere microphone strictly remains on the turntable rotation axis, nor on the loudspeaker rotation axis. To estimate the subsequent time shift in measured responses and compensate for it, we calculated for each incidence the barycentre of the arrival time of all sensors responses. The maximal time shift we found corresponds to a distance of 7mm, which has negligible impact in terms of angle error but had to be taken into account for phase correction of responses.

The loudspeaker response has been measured with a ¼ inch B&K microphone. The sensors measures were deconvolved by the loudspeaker response in order to remove its influence.

6.1.2. Diffuse field measurements

The directional sphere was not completely sampled during the free field measurements: - 90 to - 40 degrees elevation measurements were left apart due to system limitation. In order to evaluate the individual sensor response discrepancy complementary diffuse field measurements have been done in IRCAM "Espace de Projection" room.

Sensors have been measured with the same equipment than free field measurements. The logarithm sine sweep sequence was longer (18th order) to have a diffuse field in the room.

We used the Matlab "Room Analysis Toolbox" (RAT) developed by IRCAM and based on Early Decay Curve analyses. Diffuse field sensors responses were estimated on the basis on the initial power spectrum response, which is estimated by linear regression of the retrograde integration of the energy decay curve for each frequency band (short time Fourier transform on each band).

6.2. Comparison of sensors responses with the sphere diffraction model

The prototypes we built are hoped to be conform enough to the theoretical model of sphere microphone of 5 for which we've been able to define an appropriate processing. Nevertheless, such real prototypes potentially present various questionable features: sphericity, acoustic rigidity, acoustic disturbance (by the bottom sheath), radius, positioning errors, individual responses discrepancy. In the following, we present some first methods to identify and characterize deviations from the model.

For this purpose, sensors' responses have been simulated for the same wave incidences as used in measurements, accordingly to the prototype description (radius, sensors positions) of section 5. Simulations were performed from (19). Sound speed has been fixed to c=340m/s.These simulations are used as a reference basis for comparison with the measured directivity. This helps to analyze how well the measures match the model, what are the non modelled disturbances, and to detect possible positioning errors.

From this point we still use the notation introduced in 3 to describe "sphere related" *transfer functions* (instead of *signals*) with the assumption of sound fields consisting in a single plane wave. For each sensor q, we get a set of N transfer functions $s_n^q(\theta_n,\delta_n)$ associated to the N directions (θ_n,δ_n) of measurements. These compose the vector $\mathbf{s}_q$ (which might be merely noted $\mathbf{s}$). It is implicitly understood that such vectors and their elements are functions of the frequency f. We'll denote respectively by $\mathbf{s}_q^{meas}$ and $\mathbf{s}_q^{model}$ the data derived from measurement and simulation.

6.2.1. Qualitative comparison of directivities

Figure 21 shows 3D plots of sensors directivity for one sensor in the upper hemisphere (#4) and for one sensor near the sheath, below the sphere (#16). In the first case, the global directivity shape looks the same for both measured and simulated responses, even in relatively high frequency although a slight change can be observed at low elevation angles. For sensor #16, the shape is roughly respected at relatively low frequency, but the plot at 8kHz makes clearly appear the disturbance of the measured directivity caused by the sheath underneath the sphere (loss of axial symmetry compared with the model).

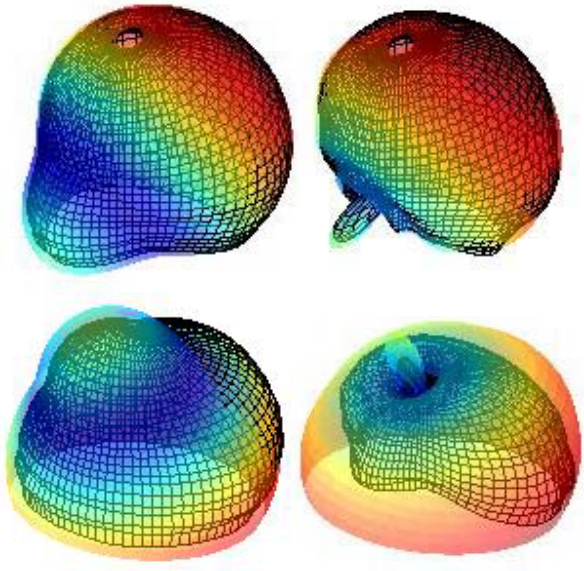

Figure 21 3D plots of measured (meshed plot) and simulated (in transparency) directivity for sensors #4 (top) and #16 (bottom) and at frequencies *f*=1kHz (left) and *f*=8kHz (right), with respect to sensor and axis positioning of Figure 18.

Figure 22 shows polar patterns at elevation=0° and for sensor #5, which is located in the horizontal plane and shouldn't be to much affected by acoustic disturbance of the bottom sheath. The global shapes of measured and simulated patterns fit rather well together. We notice that with the model, secondary lobes are always a bit greater than with the measure, while the troughs mostly coincide[2]. That means that the real prototype is slightly more directive than the model. At this point, it is hard to state whether the difference is mostly due to sheath disturbance or non strict acoustic rigidity of the sphere.

[2] We tried simulations with several values of sound speed *c* without getting a significantly better matching.

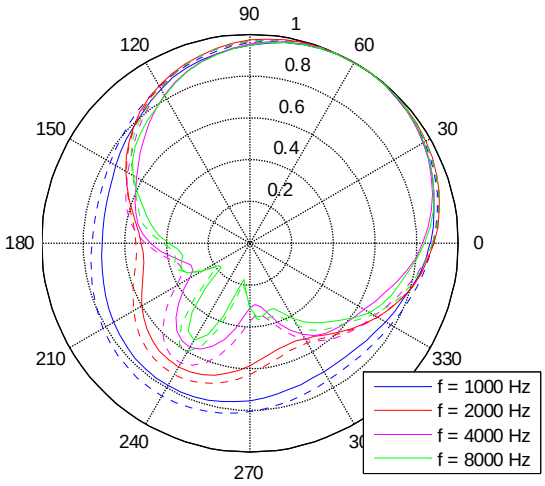

Figure 22 Polar patterns of measured (cont. lines) and simulated (dashed lines) sphere directivity for sensor #5. Directivities normalized with respect to the max values.

6.2.2. Quantitative analysis using spatial correlation

A more quantitative and global assessment of the sphere directivity model can be achieved by calculating spatial correlation between model and measure over the entire set of measurement incidences. We first compute it on the spectra modulus of sensors responses (40):

$$R_{|\mathbf{s}^{meas}|,|\mathbf{s}^{model}|} = \frac{\left\langle |\mathbf{s}^{meas}|, |\mathbf{s}^{model}| \right\rangle}{\left\| \mathbf{s}^{meas} \right\| . \left\| \mathbf{s}^{model} \right\|}, \qquad (40)$$

where we introduce the spatial scalar product and norm

$$\langle \mathbf{x}, \mathbf{y} \rangle = \mathbf{x}^{*}.\mathrm{diag}(\boldsymbol{\gamma}).\mathbf{y} \quad \text{and} \quad \|\mathbf{x}\| = \sqrt{\langle \mathbf{x}, \mathbf{x} \rangle}, \qquad (41)$$

with the vector $\boldsymbol{\gamma}$ of spatial weightings (which sum is equal to 1) to compensate for the non homogeneous distribution of measurement angles around the sphere.

The top of Figure 23 shows that values are very close (if not equal) to 1 especially at low and mid frequencies. They decrease at high frequencies especially for a few sensors. Although it's hard to state a quality judgment from absolute values, it worth noticing that the worst values concern the sensors [#10,12,15,16] near the sheath underneath the sphere, which causes a disturbing and non modelled diffraction effect.

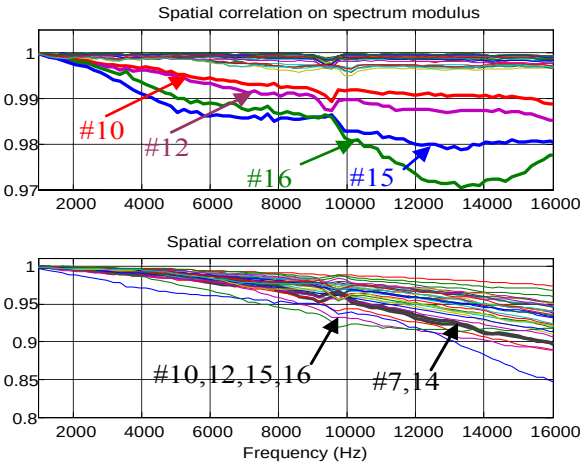

Figure 23 – Spatial correlation on spectra modulus (top) and complex spectra (bottom) between measured and simulated sensors responses.

As phase relationships are important when recombining sensors responses to form HOA directivities, it is relevant to compute spatial correlation on complex spectra (42), which includes the quality of phase matching between both modeled and measured directivity responses. For this purpose, the temporal realignment of measures as described in 6.1.1 is essential.

$$R_{\mathbf{s}^{meas},\mathbf{s}^{model}} = \frac{\left\langle \mathbf{s}^{meas}, \mathbf{s}^{model} \right\rangle}{\left\| \mathbf{s}^{meas} \right\| . \left\| \mathbf{s}^{model} \right\|} \qquad (42)$$

Bottom of Figure 23 shows that sensors #10,12,15,16 still present the worst values. It also shows *relatively* bad values for few sensors (eg #7,14) that presented a quite good directivity shape (from correlation on modulus). This is probably not due to the sheath disturbance (all the more that sensor #14 if quite elevated and far away from the sheath), but rather to a slight positioning error on the sphere that causes a shift of phase information (related to time arrival of impinging waves) over the entire sphere. As a matter of fact, a position error of roughly 1 or 1.5 mm could be visually observed for these sensors.

To summarize, spatial correlation values are globally good or very good. Nevertheless, it would be worth converting phase errors into phase delay errors in order to better identify positioning errors. Moreover, little phase errors (and therefore little complex response errors) at low frequency might be greatly amplified by microphone processing and might result in significant HOA reconstruction errors. This will be discussed in 6.3.3.

6.2.3. Extraction of individual sensors responses

In addition to directivity properties, another potential deviation of our prototypes from the theoretical model is the discrepancy between individual sensor responses. Equivalent free field response of each sensor (*i.e.* as omni directional sensor in the absence of the diffracting sphere) can be estimated together with the spatial correlation above, from the same measurements and simulations. Indeed, the measured responses can be factorized into the directivity effect and the sensor response. Provided that the measured directivity fits the model well enough (which is globally the case), equivalent free field response of a given sensor is estimated as:

$$\left| \mathbf{s}^{meas} \right| = \left| \hat{S}^{freefield} \right| . \left| \mathbf{s}^{model} \right| \qquad (43)$$

$$\left| \hat{S}^{freefield} \right| = \frac{\left\langle \left| \mathbf{s}^{meas} \right|, \left| \mathbf{s}^{model} \right| \right\rangle}{\left\| \mathbf{s}^{model} \right\|^2} \qquad (44)$$

This uses the diffraction model to spatially weight the measures and compensate for their absence in the bottom part of the directional sphere, where the bottom sensors should have their maximum response. In principle the estimation is as reliable as the calculated spatial correlation is good, which is presently the case.

We find that sensors responses are mostly parallel with a maximum level difference less than 3dB. Relative levels found between these estimations are compliant with diffuse field responses estimations discussed in 6.1.2.

6.3. Objective characterization of the HOA microphone prototype performances

6.3.1. Processing methods and computation parameters

To objectively analyse the performance of our HOA microphone prototype, we process the measured responses by means of the matrix and filters defined in 5.2, with regularisation parameters corresponding to a maximum noise amplification of resp. +0dB, +6dB and

+20dB. In order to distinguish between the limitations inherent to the model and the artefacts due to the "imperfectness" of the prototype regarding the model, we process the same way the simulated responses already involved in 6.2. We'll note $\mathbf{S} = [\mathbf{s}_1 \dots \mathbf{s}_Q]^T$ the matrix of measured (or simulated) responses and $\hat{\mathbf{B}} = [\hat{\mathbf{b}}_1 \dots \hat{\mathbf{b}}_K]^T$ the matrix of estimated HOA responses, $\hat{\mathbf{b}}_k$ being the vector of responses for all measurement directions for the of the k^{th} HOA component. HOA responses are obtained from $\hat{\mathbf{B}} = \mathbf{P}.\mathbf{S}$, with the global processing matrix:

$$\mathbf{P} = \text{diag}\left(EQ_m\right).\mathbf{E} \qquad (45)$$

Finally, to investigate the real potential of the prototype after removing the limitations caused by its discrepancy from a known model, we introduce and try another kind of processing matrix **P**. This is such that when applied on the whole set **S** of measured responses, the set of estimated HOA responses $\hat{\mathbf{B}} = \mathbf{P}.\mathbf{S}$ fits the best the HOA gains **B** expected regarding the measurement directions. This leads to a classical minimisation problem that can be solved in practice by system inversion with regularisation, as it was discussed in previous sections. The "optimal" processing matrix is computed according to the following equation:

$$\mathbf{P} = \mathbf{B}.\text{diag}(\boldsymbol{\gamma}).\mathbf{S}^*.(\mathbf{S}.\text{diag}(\boldsymbol{\gamma}).\mathbf{S}^* + \lambda\mathbf{I})^{-1}, \qquad (46)$$

where regularisation parameter λ is tuned in the same way as in 4.1.2 (but without the factor $\sqrt{Q}$) to induce the same maximum value of noise amplification. Nevertheless, parameter λ and equation (46) have to be slightly modified to ensure both a little value of noise amplification (esp. 0dB) and a correct response level. Note that this matrix is frequency dependent, *i.e.* it is a matrix of filters that is much more consuming[3] than the factorized solution in terms of digital signal processing.

In the following sections, we'll denote by **b** and $\hat{\mathbf{b}}$ the vector of resp. theoretical and estimated HOA responses. We'll use labelling (fMo+XdB) or (iMe+XdB) when referring resp. to factorized processing (45) or the solution (46), with a max noise amplification of X dB.

[3] Nevertheless we have verified that such a 32x25 filter matrix, with 256-tap FIR, can process in real time on an ordinary computer, if it is appropriately implemented.

For clearer illustrations, sensors responses have been pre-equalized to compensate their mean "free-field" response, without changing their relative levels.

6.3.2. Qualitative comparison of reconstructed and expected HOA directivities

With the aim to give a first qualitative insight into what happens in terms of HOA directivity reconstruction, we first focus on the result of the factorized processing (fMo+0dB).

Figure 24 shows 3D plots of some reconstructed directivities for 2 symptomatic frequencies. At 5 kHz, the patterns are mostly very well reconstructed (the slight amplitude mismatch will be discussed later). At 10 kHz, *i.e.* beyond the so-called spatial aliasing frequency (estimated as 7.5kHz in 5), patterns appear quite disturbed. One easily observes the presence of spherical harmonics of higher orders than the estimated ones, with sometimes a common azimuth (or elevation) dependence, presenting numerous additional lobes (higher angular frequencies). This is namely the effect of spatial aliasing.

To better assess the quality of reconstruction as a function of the frequency, let's focus on the horizontal section (0 degree elevation angle) of directivity patterns and to "horizontal" HOA components. Figure 25 shows "cylindrical views" formed by concatenating these horizontal sections along a vertical axis that represents the frequency scale. It clearly makes appear a transition frequency [band] (about 7 or 8kHz or even above depending on the order *m*) where patterns begin getting disturbed in terms of proportion between lobes and/or number of lobes. On the other side the low frequency response, which is very good for the 0^{th} component, progressively thins out over a low frequency band that enlarges as the order *m* increases. This is partly due to the quite moderated equalization effort involved in the processing here. The next section introduces quantitative criteria to further explore the reconstruction quality depending on the processing options.

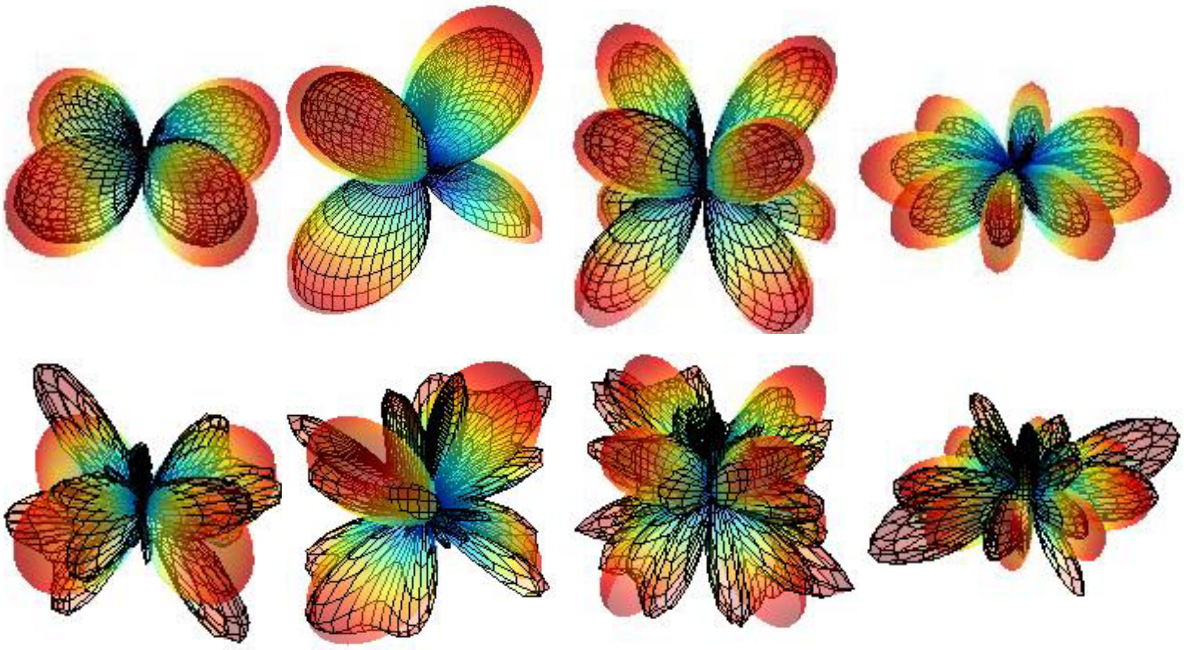

Figure 24 Reconstruction of a some specimens of HOA directivity at 5 kHz (top) and at 10 kHz (bottom). From left to right: components B_{22}^{+1}, B_{21}^{+1}, B_{32}^{+1}, B_{44}^{+1}.

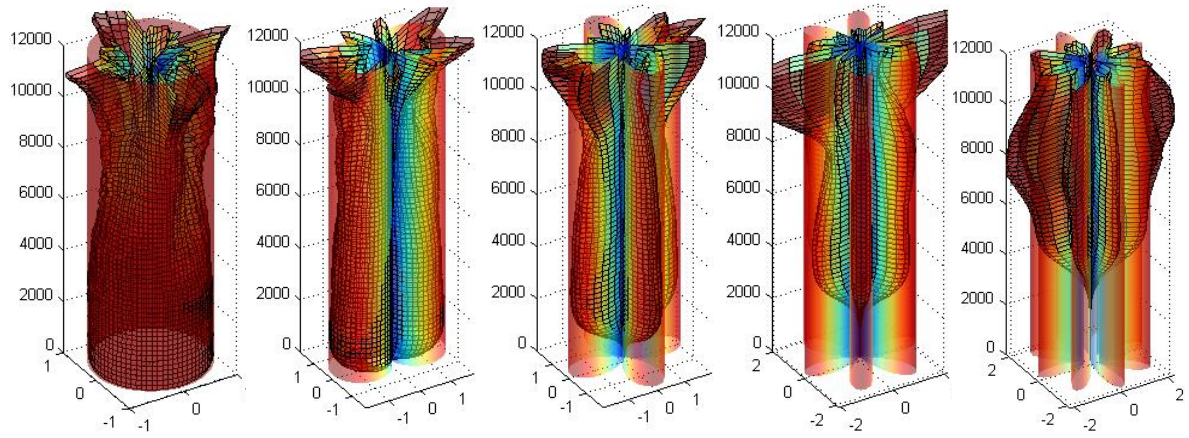

Figure 25 Cylindrical plots of reconstructed (meshed plots) and expected (in transparency) directivities for incidences in the horizontal plane, and for horizontal components B_{mm}^{+1} with m=0 to 4 (from left to right). Vertical axis is for frequency (in Hz).

6.3.3. Quantitative analysis

Similarly as in 6.2.2, we compute spatial correlation between reconstructed HOA directivities vectors $\hat{\mathbf{b}}$ and theoretical ones $\mathbf{b}$:

$$R_{\hat{\mathbf{b}},\mathbf{b}} = \frac{\left\langle \hat{\mathbf{b}}, \mathbf{b} \right\rangle}{\left\| \hat{\mathbf{b}} \right\| . \left\| \mathbf{b} \right\|} \qquad (47)$$

We complete this by a characterization of the mean level of estimated responses, relatively to the expected one:

$$L_{\hat{\mathbf{b}},\mathbf{b}} = \frac{\left\| \hat{\mathbf{b}} \right\|}{\left\| \mathbf{b} \right\|} \qquad (48)$$

These equations indicates that in the case of factorized processing, the post-equalization has an impact of the component level (*i.e.* the scale of directivity response), but none on spatial correlation (*i.e.* the respect of the directivity "shape").

Both a good spatial correlation and a correct level of estimated HOA components take part into the quality of the captured sound field representation, and therefore of its reconstruction at the final rendering stage (after spatial decoding) 2.1.3.

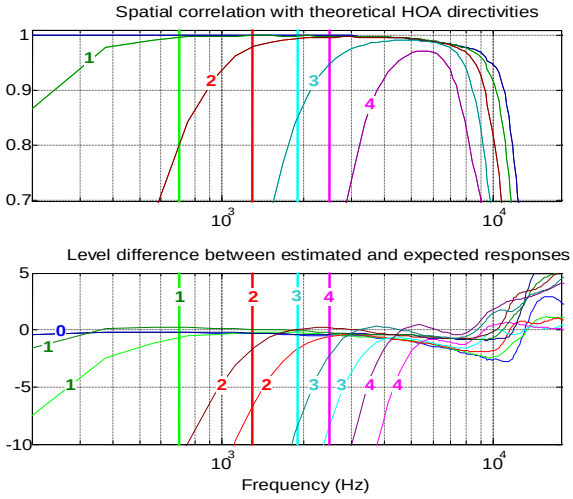

Figure 26 Quality of reconstructed directivity when processing is applied to measures. For more readability, each group of m^{th} order components is represented by a single, mean curve. Vertical bars correspond to limit frequencies (700, 1300, 1900, 2500 Hz) corresponding to 1st, 2nd, 3rd, and 4th order rendering, as computed in 2.1.3. For bars and curves, 0th, 1st, 2nd, 3rd, and 4th orders are respectively represented in blue, green, red, cyan, and magenta, and appear from left to right. Component levels (bottom) corresponding to amplification parameters +0dB, +6dB resp. appear from right to left while darkening in color.

Figure 26 shows curves computed for measures processed with (fMo+0dB) (fMo+6dB) options. The case (fMo+20dB) is not plotted here to avoid confusion. In the present case, correct spatial correlation is bounded by both low and high frequency limits, the former being as high as the order. For comparison, Figure 27 shows the case of responses obtained from simulation. Since no errors are introduced in simulations with regard to the model, spatial correlation is perfect from 0Hz to the spatial aliasing frequency 7.5 kHz and even above (as the order decreases).

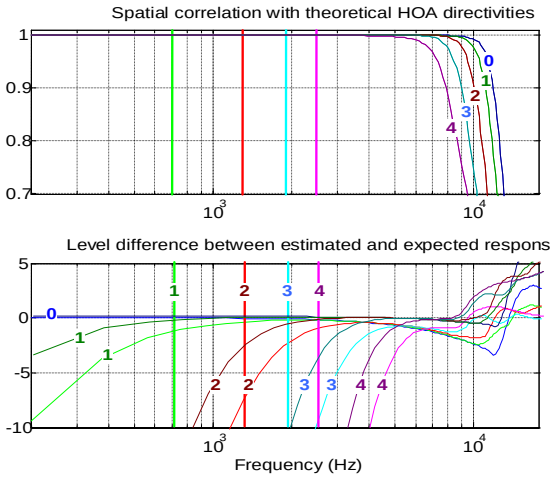

Figure 27 Same as Figure 26 but for processing applied to simulations.

Relative levels of estimated components look very similar in both cases (measures and simulations). They are approximately flat over a frequency band (also bounded by the spatial aliasing frequency) that extends towards low frequencies as much as the order is low and as the equalisation effort is high. With a +20dB allowed noise amplification, the lower bound of the "correct level frequency band" reaches the limit frequencies shown as vertical bars, even for 3rd and 4th orders. Nevertheless, there is no use to invest such an equalization effort (at least for the 4th order components) when dealing with the real prototype, for which the frequency band of potentially good reconstruction is

bounded by the low frequency slope of spatial correlation curves: Top of Figure 26 shows that good correlation is not reached at the limit frequency for the 4th order. As a general rule, there's no use that the frequency band of correct level exceeds the frequency band of correct spatial correlation.

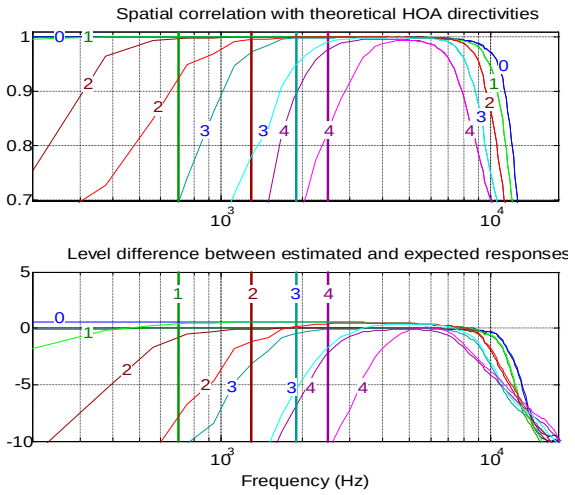

Figure 28 Same as previous figures, but with optimised processing (iMe+6dB) and (iMe+20dB) applied to measures.

Another useful comparison can be done with the HOA estimation derived from the processing labelled (iMeXdB) (Figure 28), which is optimized from the whole set of measurements (46). With the same given estimation effort, it presents roughly the same features as above in terms of maximal noise amplification and relative level of estimated components (except above the spatial aliasing frequency). It presents a spatial correlation that improves with higher estimation effort similarly to the component level. That means that with a more complete knowledge of the prototype's real directivity, one is able to reach HOA reconstruction properties as good as with model-based simulations.

6.3.4. Energy vector analysis

To complete the analysis of the prototype microphone performances, we anticipate now another feature of the spatialisation effect observed at the final rendering stage: that is a localisation criterion called "energy vector", introduced and discussed in 2.1.3. We compute it by operating a 4th order, "max r_E" decoding over estimated HOA frequency responses. It is considered to be a relevant localisation criterion in the medium-high frequency band where acoustic reconstruction at the listener scale is no longer satisfied.

Energy vector characteristics are drawn as functions of the frequency in Figure 29 (bottom part): its mean angle error regarding the expected directions (*i.e.* the measurement directions) and the "blur width angle" α_E computed from its mean norm.

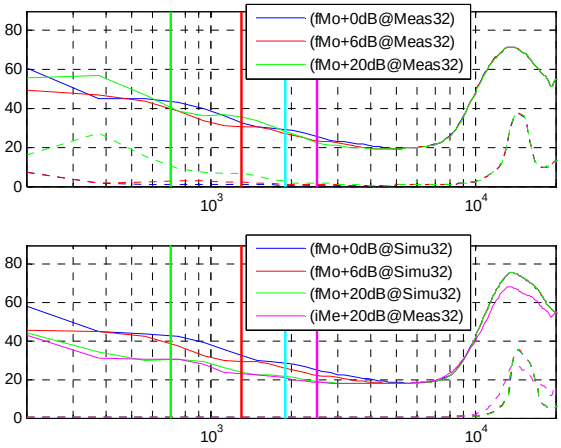

Figure 29 Global quality of energy vector at the reproduction stage: mean angle error regarding the expected directions (dashed lines); "blur width angle" α_E (cont. lines). All angles are in degrees.

In almost all cases, the angle error is approximately null up to the supposed spatial aliasing frequency and even beyond (about 10 kHz). The "blur angle" (attached to the vector norm) is quite important at low frequencies. It reaches its minimal value at about 5-6 kHz: that is also nearly the "optimal" value given by Table 1 for M=4, *i.e.* 18 degrees. It increases again from the spatial aliasing frequency and reaches a maximum of 70 degrees above 10 kHz.

In the case of factorized processing of measures (Top of the figure), it appears that a +6dB estimation effort reduces the "blur angle" just a bit (from 5 to 10 degrees). Curves confirm that a +20dB effort is counterproductive: blur angle as well angle error are greater at low frequency. On the contrary, increasing efforts are fruitful when applied to the simulated responses, as the bottom figure shows it (about 15 degrees blur angle reduction). Finally, optimised measures processing competes with processing on simulated responses for the same effort (+20dB on the figure).

7. CONCLUSION

This study completes an investigation work done by present authors as well as concurrent teams for some years on 3D sound field recording with microphone arrays, especially in relation with the spatialisation approach called "Higher Order Ambisonics". Focussing on spherical arrays, this work has led to the construction of a 4th order, 32 sensor microphone prototype and the design of appropriate signal processing methods grounded on both theoretical and practical considerations.

To objectively assess the performance of this HOA microphone as an efficient tool for spatially encoding natural sound fields, we performed complete directivity measurements and analysis. We proposed and discussed objective criteria like the spatial correlation between estimated HOA directivities with the expected spherical harmonics. The relevance of the encoding with regard to the sound field reproduction stage has also been discussed using the energy vector criterion. As a result, the prototype presents a nice potential as a 3D sound field recording means with moderate amplification effort. Further improvements are expected from this study.

Now a complete HOA spatialisation chain can be demonstrated, featuring 3D recording, virtual source encoding, sound field manipulations and spatial decoding, with signal processing modules implemented *e.g.* as VST plug-ins. As a particular example, real time HOA recording, processing and decoding for ITU loudspeaker setup as well as for a head-tracked binaural rendering, have been successfully demonstrated at the "*Journées d'Etudes sur la Spatialisation*" (JES2006) that took place at IRCAM and ENST-Paris in January 2006.

8. ACKNOWLEDGEMENTS

The authors would like to thank Olivier Warusfel for his valuable help in the objective microphones measurements done in IRCAM and for the room analysis toolbox.

9. REFERENCES

[1]. GERZON, M.A., *Periphony: With-Height Sound Reproduction.* J. Audio Eng. Soc., 1973. **21**(1): p. 2-10.

[2]. BAMFORD, J.S., *An Analysis of Ambisonics Sound Systems of First and Second Order*. 1995, Université de Waterloo: Waterloo.

[3]. DANIEL, J., *Représentation de champs acoustiques, application à la transmission et à la reproduction de scènes sonores complexes dans un contexte multimédia*. 2001, Paris 6: Paris.

[4]. DANIEL, J., NICOL, R., and MOREAU, S. *Further Investigations of High Order Ambisonics and Wavefield Synthesis for Holophonic Sound Imaging*. in *114th AES Conv.* 2003. Amsterdam, The Netherlands.

[5]. CRAVEN, P. and GERZON, M.A., *Coincident Microphone Simulation Covering Three Dimensional Space and Yielding Various Directionnal Outputs*. 1977: U.S.

[6]. ABHAYAPALA, T.D. and WARD, D.B. *Theory and Design of Higher Order Sound Field Microphones Using Spherical Microphone Array*. in *IEEE ICASSP '02*. 2002.

[7]. DURAISWAMI, R., et al. *High Order Spatial Audio Capture and its Binaural Head-Tracked Playback over Headphones with HRTF Cues*. in *AES 119th Convention*. 2005. New York, NY, USA.

[8]. GOVER, B.N., RYAN, J.G., and STINSON, M.R., *Measurements of directional properties of reverberant sound fields in rooms using a spherical microphone array.* J. Acoust. Soc. Am., 2004. **116**(4, Pt. 1): p. 2138-2148.

[9]. MEYER, J. and AGNELLO, T. *Spherical microphone array for spatial sound recording*. in *AES 115th Conv.* 2003. New York, NY, USA.

[10]. MOREAU, S. and DANIEL, J. *Study of Higher Order Ambisonic Microphone*. in *joint meeting cfa-daga '04*. 2004. Strasbourg, France.

[11]. MOREAU, S., DANIEL, J., and CHRAA, A. *Production, transmission et restitution temps réel d'une scène sonore dans un format audio 3D flexible*. in *CORESA 2004*. 2004. Lille.

[12]. RAFAELY, B., *Analysis and Design of Spherical Microphone Arrays.* IEEE Transaction on Speech and Audio Processing, 2005. **13**(1): p. 135-143.

[13]. LABORIE, A., BRUNO, R., and MONTOYA, S. *A New Comprehensive Approach of Surround Sound Recording*. in *AES 114th Conv.* 2003. Amsterdam, The Netherlands: AES.

[14]. DANIEL, J. and MOREAU, S. *Further Study of Sound Field Coding with Higher Order Ambisonics*. in *AES 116th Conv.* 2004. Berlin, Germany: AES.

[15]. GERZON, M.A., *Ambisonics in Multichannel Broadcasting and Video.* J. Audio Eng. Soc., 1985. **33**(11): p. 859-871.

[16]. DANIEL, J., RAULT, J.B., and POLACK, J.D. *Ambisonics Encoding of Other Audio Formats for Multiple Listening Conditions*. in *AES 105th Conv.* 1998.

[17]. MALHAM, D. *Experience With Large Area 3-D Ambisonic Sound Systems*. in *Proc. of the Institute of Acoustics*. 1992.

[18]. MORSE, P.M. and INGARD, K.U., *Theoretical Acoustics*. Mc Graw-Hill ed. 1968, New York.

[19]. WARD, D.B. and ABHAYAPALA, T.D., *Reproduction of a Plane-Wave Sound Field Using an Array of Loudspeakers.* IEEE Transaction on Speech and Audio Processing, 2001. **9**(6): p. 697-707.

[20]. ELKO, G. and NGUYEN PONG, A.-T. *A steerable and variable first-order differential microphone*. in *Proc. 1997 IEEE ICASSP*. 1997.

[21]. LI, Z. and DURAISWAMI, R. *A Robust and Self-Reconfigurable Design of Spherical Microphone Array for Multi-Resolution Beamforming*. in *IEEE ICASSP '05*. 2005.

[22]. GOLUB, G. and VAN LOAN, C., *Matrix Computations, third edition*. 1996, London: The Johns Hopkins University Press.

[23]. TIKHONOV, A.N. and ARSENIN, V.A., *Solution of Ill-posed Problems*. 1977, Washington: Winston & Sons.

[24]. KIRKEBY, O. and NELSON, P.A., *Fast Deconvolution of Multi-Channel Systems using Regularisation*. 1996, ISVR Technical Report no.255: Southampton, UK.

[25]. DRISCOLL, J.R. and HEALY, D.M., *Computing Fourier Transforms and Convolutions on the 2-Sphere.* Adv. Appl. Math., 1994. **15**: p. 202-250.

[26]. ARFKEN, G., *Mathematical Methods for Physicists, 3rd ed.* 1985, San Diego, CA: Academic Press.

[27]. VERHAEVERT, J., VAN LIL, E., and VAN DE CAPELLE, A. *Uniform Spherical Distributions For Adaptive Array Applications*. in *VTC'01*. 2001: IEEE.

[28]. SLOANE, N.J.A., and al., *Spherical Codes*. http://www.research.att.com/~njas/packings/

[29]. FLIEGE, J., *Integration nodes for the sphere*. http://web.mat.bham.ac.uk/J.Fliege/nodes/nodes.html